Langmuir

Article

pubs.acs.org/Langmuir

Electrostatically Anchored Branched Brush Layers

Xiaoyan Liu,[†] Andra Dedinaite,[†,‡] Mark Rutland,[†,‡] Esben Thormann,*[,†] Ceslav Visnevskij,[§] Ricardas Makuska,[§] and Per M. Claesson[†,‡]

[†]Department of Chemistry, Surface and Corrosion Science, School of Chemical Sciences and Engineering, KTH Royal Institute of Technology, Drottning Kristinas väg 51, SE-100 44 Stockholm, Sweden

[‡]Institute for Surface Chemistry, P.O. Box 5607, SE-114 86 Stockholm, Sweden

[§]Department of Polymer Chemistry, Vilnius University, Naugarduko 24, LT-03225 Vilnius, Lithuania

Supporting Information

ABSTRACT: A novel type of block copolymer has been synthesized. It consists of a linear cationic block and an uncharged bottle-brush block. The nonionic bottle-brush block contains 45 units long poly(ethylene oxide) side chains. This polymer was synthesized with the intention of creating branched brush layers firmly physisorbed to negatively charged surfaces via the cationic block, mimicking the architecture (but not the chemistry) of bottle-brush molecules suggested to be present on the cartilage surface, and contributing to the efficient lubrication of synovial joints. The adsorption properties of the diblock copolymer as well as of the two blocks separately were studied on silica surfaces using quartz crystal microbalance with dissipation monitoring (QCM-D) and optical reflectometry. The adsorption kinetics data highlight that the diblock copolymers initially adsorb preferentially parallel to the surface with both the cationic block and the uncharged bottle-brush block in contact with the surface. However, as the adsorption proceeds, a structural change occurs within the layer, and the PEO bottle-brush block extends toward solution, forming a surface-anchored branched brush layer. As the adsorption plateau is reached, the diblock copolymer layer is 46−48 nm thick, and the water content in the layer is above 90 wt %. The combination of strong electrostatic anchoring and highly hydrated branched brush structures provide strong steric repulsion, low friction forces, and high load bearing capacity. The strong electrostatic anchoring also provides high stability of preadsorbed layers under different ionic strength conditions.

1. INTRODUCTION

Bottle-brush molecular constructs, such as mucins, lubricins, and aggrecan−hyaluronan complexes,[1,2] fulfill many important biological functions related to protection, hydration, and lubrication. Mucins and lubricins consist of a polypeptide backbone to which a large number of oligosaccharide side chains are attached. In many types of mucins and lubricinsone or several globular polypeptide domains are found at the C and/or N terminal region,[3−5] and in many cases they serve to anchor the bottle-brush polymers to biointerfaces.[6,7] The aggrecan−hyaluronan complex consists of a polysaccharide backbone (hyaluronan) to which a large number of bottle-brush glycoproteins (aggrecan) are attached with the aid of a link protein.[8] Characteristics of these molecules include high molecular weight polydispersity and highly hydrated and often anionic side chains. It has been suggested,[9] but to our knowledge not proven, that bottle-brush molecules are anchored to the cartilage surface exposing their heavily glycosylated region in a preferential perpendicular orientation to the cartilage/synovial fluid interface.

The wide use of bottle-brush molecules by nature has inspired considerable interest in synthetic bottle-brush polymers. In particular, random copolymer bottle-brush polymers, consisting of one type of segment that carries a positive charge and another type of segment that carries a nonionic and hydrophilic side chain, have found considerable interest as lubricants.[10,11] The chemistry of bottle-brush glycoproteins and synthetic bottle-brushes are, however, quite different. In particular, the side chains of the glycoproteins are built by carbohydrates, where anionic ones are abundant. By contrast, the side chains of the synthetic alternatives are often made of nonionic and strongly hydrated poly(ethylene oxide) (PEO) side chains.[12,13]

The rationale for making the synthetic random copolymer brushes into cationic polyelectrolytes is that many relevant surfaces of use in technology and science, e.g., most oxides and mica, are negatively charged. Thus, electrostatic interactions can be used for driving the cationic random bottle-brush polymers to adsorb to the surface. The preference for using PEO side chains is related to their high hydration and hydrophilic nature at not too high temperatures,[14,15] which makes PEO into an efficient steric stabilizer for many types of colloidal particles.[16]

Adsorbed layers formed by the cationic random bottle-brush copolymers with PEO side chains have shown many useful features. For instance, they can be used for achieving low protein adsorption,[17−19] strong steric repulsion,[10] and low frictional forces[10,11] providing the number of PEO side chains per unit area brought to the solid−liquid interface is sufficiently

Received: July 18, 2012
Revised: September 3, 2012
Published: October 9, 2012

Table 1. Number and Weight Average Molecular Weight, M_n and M_w, Respectively, Number Average Degree of Polymerization, DP, Apparent Diffusion Constant, D_{app}, and Hydrodynamic Radius, R_H, of the Cationic Polymer $(METAC)_m$, the Bottle-Brush Polymer $(PEO_{45}MEMA)_n$, and the Diblock Copolymer $(METAC)_m$-*b*-$(PEO_{45}MEMA)_n$

polymer	$M_n \cdot 10^{-3}$	$M_w \cdot 10^{-3}$	M_w/M_n	DP	D_{app} (m^2/s)	R_H (nm)
$(METAC)_m$	18.7	23.4	1.25	90	6.2×10^{-11}	4
$(PEO_{45}MEMA)_n$	236	871	3.69	113	1.2×10^{-11}	21
$(METAC)_m$-*b*-$(PEO_{45}MEMA)_n$	235	698	3.01	90 + 102	1.1×10^{-11}	22

high. Recently, theoretical modeling has been utilized for gaining insight into adsorption properties of cationic bottle-brush polymers with PEO side chains, and how these are affected by the architecture of the polymer. In particular, the modeling results predicted that especially high adsorbed amounts and extended layers could be formed if the side chains were clustered at one end of the polymer chain, forming a diblock copolymer consisting of a charged block and a nonionic bottle-brush block.[20]

The bottle-brush polymer that was used in this study differs from the ones used in previous work in that it is a *diblock copolymer* rather than a random copolymer. The design criteria for the synthesis was based on the following:

(i) The polymer should adsorb strongly to negatively charged surfaces, and for this reason a cationic anchor block was used.

(ii) The side chains should be able to generate strongly repulsive forces, and 45 unit long PEO chains have previously been shown to achieve this.[10,15] Thus, such side chains were used also in this case.

(iii) Theoretical modeling has predicted that cationic diblock bottle-brush structures adsorb to larger amounts than cationic random bottle-brush structures.[20,21]

(iv) It has been suggested that biological bottle-brush molecules are oriented preferentially perpendicular to the cartilage surface and whereby aid lubrication.[9] Modeling suggests[20,21] that such a structure can be achieved more efficiently by using diblock bottle-brushes, rather than the random bottle-brushes used so far. Indeed, the lowest friction coefficients reported for random bottle-brush polymers were obtained for adsorbed layers where the bottle-brush structure was partly oriented away from the surface.[10]

(v) The bottle-brush polymers found in nature are typically highly polydisperse.[6] Thus, a significant polydispersity of the bottle-brush block in the cationic diblock bottle-brush structure is not regarded as a disadvantage for the lubrication properties.

The synthesized diblock copolymer consists of a cationic block of methacryloxyethyl trimethylammonium chloride (METAC) and an uncharged bottle-brush block of poly(ethylene oxide)methylether methacrylate ($PEO_{45}MEMA$). This polymer will be referred to as $(METAC)_m$-*b*-$(PEO_{45}MEMA)_n$. The adsorption of this diblock copolymer onto silica surfaces was investigated by optical reflectometry and quartz crystal microbalance with dissipation monitoring (QCM-D), and compared to the adsorption behavior of each of these blocks separately. The ability of the formed layers to generate steric interactions and low friction forces were also probed by employing the atomic force microscope (AFM) colloidal probe technique.

2. MATERIALS AND METHODS

2.1. Materials. Sodium chloride (NaCl, BioXtra, ≥99.5%) was purchased from Sigma-Aldrich and used as received. Water was purified by employing a Milli-ROPls unit connected to a Milli-Q plus 185 system, and filtered through a 0.2 μm Millipak filter. The resistivity of the purified water was 18.2 MΩcm, and the organic content was less than 3 ppb.

Thermally oxidized silicon wafers with a 100 nm thick SiO_2 layer from Wafer Net, Germany, were used in optical reflectometry measurements. The wafers were cut to size and cleaned by immersion in 2 wt % Hellmanex (Hellma GmbH) solution for 30 min followed by rinsing several times with Milli-Q water. The wafers were left overnight in Milli-Q water before measurement. AT-cut silica crystals with 5 MHz fundamental frequency from Q-sense, Gothenburg, Sweden, were used for QCM-D measurements. The silica crystals were cleaned using the same procedure as for the thermally oxidized silicon wafers.

2.2. Synthesized Polymers. The synthesis route for the diblock polymer used in the present investigation is provided in the Supporting Information. The different polymers were characterized by ^{1}H NMR spectroscopy, size exclusion chromatography (SEC) and dynamic light scattering (DLS), and details are provided in the Supporting Information. The SEC and DLS data are summarized in Table 1.

The DP of $(METAC)_m$ calculated from the M_n value is consistent with the ratio of the monomer to the initiator and the monomer conversion and equals 90. The polydispersity index of this polymer is 1.25. The degree of polymerization, DP, of $(PEO_{45}MEMA)_n$ calculated from M_n is about 110, and that of the $(PEO_{45}MEMA)_n$ block in the block copolymer $(METAC)_m$-*b*-$(PEO_{45}MEMA)n$ is approximately 100. Thus, the average DP of the two blocks in the copolymer $(METAC)_m$-*b*-$(PEO_{45}MEMA)_n$ is almost the same. The ratio between M_w and M_n is large, showing that the $(PEO_{45}MEMA)_n$ block is polydisperse, and the length of this block is different in individual polymer chains. This situation is similar to what is found in biological bottle-brush molecules, e.g., mucins, lubricins, and hyaluronan–aggrecan complexes,[1,2] which provide protection, hydration, and lubrication of many internal biological surfaces. Thus, the large polydispersity of the bottle-brush block is similar to that found in natural bottle-brush polymers. However, the polydispersity effect on adsorption has to be considered. It has been shown that the total adsorption energy per unit area in the system is not strongly affected by the polydispersity,[22] but there is, for entropic reasons, a strong accumulation of the high molecular compounds at the interface.[23]

2.3. Methods. *2.3.1. Optical Reflectometry.* The adsorption of the polymers on thermally oxidized silicon wafers was investigated by optical reflectometry.[24] Stagnation point adsorption reflectometry experiments were performed in a temperature-controlled room at 25 ± 1 °C. Linearly polarized light is reflected on the SiO_2/Si-water interface at an angle close to the Brewster angle. The reflected light is split into its parallel and perpendicular polarization components, I_p and I_s, and the respective intensities are recorded by photodiodes. The ratio I_p/I_s, which is defined as the signal (S), is continuously recorded during the experiment. The change in the signal (ΔS) upon adsorption is related to the adsorbed amount, Γ_{refl}, via[24]

$$\Gamma_{refl} = \frac{1}{A_S} \times \frac{\Delta S}{S_o} \quad (1)$$

The parameter A_s, also known as the sensitivity factor (relative change in S per unit adsorbed amount), can be determined by treating

dx.doi.org/10.1021/la3028989 | Langmuir 2012, 28, 15537−15547

the system as a four-layer optical model where each layer is characterized by its thickness (t), and refractive index (n): Si (n_{Si}, t_{Si})−SiO_2 (n_{SiO2}, t_{SiO2})−adsorbing layer (n_{layer}, t_{layer})−aqueous medium (n_{water}) within the framework of the Fresnel reflectivity theory.[25] It can also be determined experimentally using the procedure suggested by Dedinaite,[26] and this method was applied here. It requires knowledge of the refractive index increments, dn/dc, which were determined with an interferometric refractometer, Optilab DSP from Wyatt technology. The values obtained in the absence of added salt for $(METAC)_m$, $(PEO_{45}MEMA)_n$, and $(METAC)_m$-b-$(PEO_{45}MEMA)_n$ were 0.158, 0.142, and 0.145 mL/g, respectively. The value of dn/dc of the diblock copolymer was insignificantly affected by the NaCl concentration, and in 100 mM NaCl it was measured to be 0.1445 mL/g.

2.3.2. QCM-D. QCM-D measurements were performed using a Q-sense E4 microbalance (Q-sense, Gothenburg, Sweden). The resonance frequency (f) and the energy dissipation (D) of the crystal are accurately determined as described by Rodahl et al.[27] The dissipation is measured by switching off the driving power to the sensor and monitoring the amplitude decay profile of the oscillator. The signal decays as an exponentially damped sinusoidal function with a characteristic decay time (τ). The decay time is related to the dissipation by

$$D = \frac{2}{\omega\tau} \tag{2}$$

$$D = \frac{1}{Q} = \frac{E_D}{2\pi E_S} \tag{3}$$

where ω is the angular frequency, Q is the quality factor, E_D is the energy dissipated, and E_S is the energy stored in one oscillation, respectively. The frequency change (Δf) and the dissipation change (ΔD) were recorded using the Q-tools program (Q-sense, Gothenburg). In order to convert the measured quantities to, e.g., mass, a model has to be invoked, and several different ones have been suggested in the literature.[28−30] In this work we employed the Sauerbrey model when rigid layers were formed, and the Voigt model for viscoelastic layers.

2.3.2.1. The Sauerbrey Model. The Sauerbrey model[28] assumes that the frequency change only depends on the mass attached to the crystal ($\Gamma_{QCM\text{-}D}$) as described by the expression:

$$\Gamma_{QCM\text{-}D} = \frac{-C \times \Delta f}{n} \tag{4}$$

where n is the overtone number, Δf is the frequency change, and C is a constant that is a characteristic for a specific type of QCM-D crystal. In our case, the value of C is 0.177 mg m^{-2} Hz^{-1}. The above equation is accurate for rigid films, i.e., when the change in dissipation is small, and this model was employed when evaluating the data obtained for the cationic block. This model is not appropriate for more viscoelastic layers, and for that reason we employed the Voigt model when analyzing QCM-D data obtained for the nonionic bottle-brush block and for the diblock copolymer.

2.3.2.2. The Voigt Model. In the Voigt model, the frequency change and the dissipation change are related to the viscoelastic properties of the adsorbed film via the β-parameter,[30] given as

$$\Delta f = \mathrm{Im}\left(\frac{\beta}{2\pi t_q \rho_q}\right) \tag{5}$$

$$\Delta D = -\mathrm{Re}\left(\frac{\beta}{\pi f t_q \rho_q}\right) \tag{6}$$

where the β-parameter introduced in this model is analogous to the complex impedance (Z^*) used in the Johannsmann model.[29] The β-parameter contains information on the viscoelasticity of the adsorbed film.

A relevant viscoelastic model should be chosen to describe the adsorbed film for relating the β-parameter to the viscoelastic quantities (such as elasticity and viscosity). In this respect, the adsorbed film is modeled as a Voigt solid, in which the total stress acting on the material is the sum of stresses due to elastic and viscous effects, given as

$$\sigma_{xy} = \mu_f \frac{\partial u_x(y,t)}{\partial y} + \eta_f \frac{\partial v_x(y,t)}{\partial y} \tag{7}$$

The first term is Hooke's law, where μ_f denotes the shear elasticity modulus of the adsorbed film, and u_x refers to displacement in the x direction. The second term is Newton's law in which η_f denotes the shear viscosity of the adsorbed film, and ν_x refers to the velocity in the x direction.

In the Voigt model, the adsorbed film of thickness d_f and density ρ_f is characterized by a complex shear modulus μ^*:

$$\mu^* = \mu' + i\mu'' = \mu_f + i2\pi f\eta_f = \mu_f(1 + i2\pi f\tau) \tag{8}$$

where μ_f is the elastic shear modulus, η_f is the shear viscosity, and $\tau = \eta_f/\mu_f$ is the characteristic relaxation time of the adsorbed film.

The β-parameter is obtained by solving the wave equation for bulk shear waves propagating in a medium whose viscoelasticity is described by a Voigt model. The expression for a single viscoelastic layer in a liquid medium is given as

$$\Delta f = -\frac{1}{2\pi t_q \rho_q}\left\{d_f\rho_f\omega - 2d_f\frac{\eta_f\omega^2}{\mu_f + \omega^2\eta f^2}\left(\frac{\eta_b}{\delta}\right)^2\right\} \tag{9}$$

$$\Delta D = \frac{1}{2\pi f t_q \rho_q}\left\{2d_f\frac{\eta_f\omega}{\mu_f{}^2 + \omega^2\eta_f^2}\left(\frac{\eta_b}{\delta}\right)^2\right\} \tag{10}$$

where all symbols have the same meaning as before. The subscript "b" denotes the bulk liquid, and δ is the viscous penetration depth defined as

$$\delta = \sqrt{\frac{2\eta_b}{\rho_b\omega}} \tag{11}$$

In the analysis of the data, the frequency and dissipation changes are fitted by eqs 9 and 10, respectively.

The water content of the adsorbed layer was calculated by combining the adsorbed mass determined from optical reflectometry and the sensed mass measured by QCM-D as

$$\%\mathrm{water} = \frac{\Gamma_{QCM\text{-}D} - \Gamma_{refl}}{\Gamma_{QCM\text{-}D}} \times 100 \tag{12}$$

The effective hydrodynamic thickness of the adsorbed layer was calculated according to eq 13:

$$d_{eff} = \frac{\Gamma_{QCM\text{-}D}}{\rho_{eff}} = \frac{\Gamma_{QCM\text{-}D}}{\left[\rho_{polymer} \times \frac{\Gamma_{refl}}{\Gamma_{QCM\text{-}D}}\right] + \rho_{water} \times \left[1 - \frac{\Gamma_{refl}}{\Gamma_{QCM\text{-}D}}\right]} \tag{13}$$

where d_{eff} is the effective hydrodynamic thickness of the adsorbed layer, and $\rho_{polymer}$ is the bulk density of the polymer.[31] The use of eqs 12 and 13 relies on the assumption of insignificant volume change of mixing. A value for the layer thickness, d_{Voigt}, was also obtained directly from the Voigt model.

2.3.3. AFM. Force and friction measurements were performed in a fused silica liquid cell (volume around 0.1 mL), using a Multimode Nanoscope III Pico Force AFM (Bruker). Rectangular tipless cantilevers (NSC 12, MikroMasch, Madrid, Spain) with the approximate dimensions of 350 μm in length, 35 μm in width, and normal spring constants in the range 0.2−0.7 N/m were used. The exact values of the spring constants (normal and torsional) before attachment of the colloidal probe were determined by the Sader method.[32,33] The thermal frequency spectra of the cantilevers were measured at room temperature without any particles attached. The

dx.doi.org/10.1021/la3028989 | Langmuir 2012, 28, 15537−15547

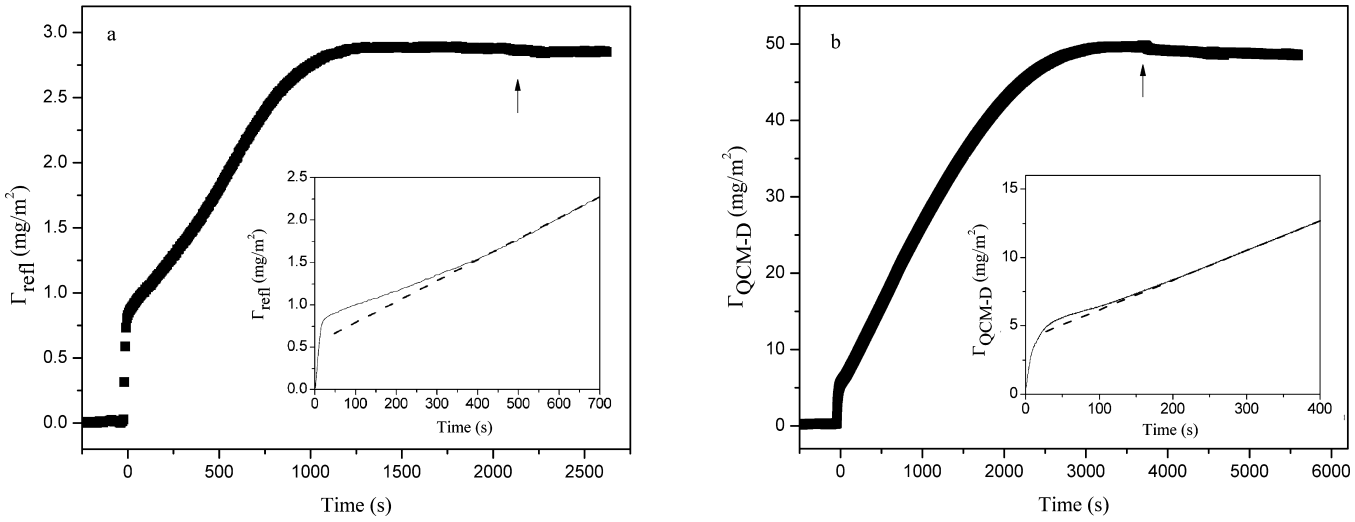

Figure 1. (a) Adsorbed mass and (b) sensed mass, calculated from overtone 3, as a function of time during adsorption of $(METAC)_m$-*b*-$(PEO_{45}MEMA)_n$ on silica from water (pH ∼ 6). The diblock copolymer at a concentration of 50 ppm was injected at time = 0. The arrows mark the start of the rinsing process with Milli-Q water. The insets focus on the initial adsorption, and the dashed lines in the insets are provided to emphasize the increase in adsorption rate that occurs after a few hundred seconds.

lateral photodetector sensitivity, δ (V rad^{-1}), was calibrated using the method of tilting the AFM head as suggested by Petterssonet al.[34] The silica colloidal probes with diameter of approximately 20 μm in diameter were attached to the end of the cantilever with the aid of an Eppendorf Micromanipulator 5171, a Nikon Optiphot100S reflection microscope, and a small amount of epoxy glue (Araldite, 80806). The size of the particles was determined using a Nicon Optiphot 100S reflection microscope, employing image analysis with National Instrument Vision Assistant 8.0.

Before each experiment, the fused silica liquid cell and all other tools were cleaned by immersion in 2 wt % Hellmanex (Hellma GmbH) solution for about 1 h. They were rinsed several times by Milli-Q water and blow-dried with filtered nitrogen gas.

The normal surface forces were measured with a constant approach and retraction speed of 2 μm/s. The friction measurements were performed by sliding the surfaces backward and forward 10 times at each normal load and registering the cantilever twist angle. The sliding distance was 1 μm in each direction, and the scan rate was 1 Hz, giving a sliding speed of 2 μm/s.

3. RESULTS

The result section is built as follows: First we discuss how the adsorbed layer of $(METAC)_m$-*b*-$(PEO_{45}MEMA)_n$ evolves as the polymer adsorbs to silica from water. In the following section, the adsorbed layer of $(METAC)_m$-*b*-$(PEO_{45}MEMA)_n$ is considered after adsorption equilibrium has been reached, and the properties of the layer formed by the diblock copolymer is compared to those of layers formed by the individual blocks of the copolymer. In the following section, we elucidate how the ionic strength of the solution during adsorption affects the adsorbed layer. This is followed by a paragraph describing how a change in ionic strength affects layers preadsorbed from water, and in the final result section we demonstrate strong steric repulsion and low frictional forces between silica surfaces coated by $(METAC)_m$-*b*-$(PEO_{45}MEMA)_n$.

3.1. Kinetic Aspects of Layer Formation. The adsorption of $(METAC)_m$-*b*-$(PEO_{45}MEMA)_n$ on silica surfaces was followed in real time using optical reflectometry and QCM-D. The results, which are illustrated in Figure 1, demonstrate complex adsorption kinetics. The fast initial adsorption is followed by a region where the adsorbed amount increases slowly toward that corresponding to a monolayer oriented parallel to the surface. After this, the adsorption rate increases again due to reorientation of the adsorbed polymer, until it slows down again as the plateau adsorbed amount for the extended conformation of the polymer is approached. Rinsing with water results in very limited desorption.

The sensed mass determined with QCM-D, which includes the mass of the polymer and the mass of water that is hydrodynamically coupled to the layer, evolves in a similar fashion as the adsorbed amount. We note that the sensed mass is an order of magnitude larger than the adsorbed amount, which reflects the high water content of the layer. Due to the different flow conditions in the two instruments, the adsorption kinetics cannot be directly compared.

The *increase* in adsorption kinetics that is observed after a few hundred seconds is not typical for polymer adsorption and indicates that a structural change in the adsorbed layer takes place.[35,36] This change can conveniently be illustrated by the QCM-D data, by plotting the change in dissipation as a function of the change in frequency. Such plots for $(METAC)_m$-*b*-$(PEO_{45}MEMA)_n$ and for the nonionic block, $(PEO_{45}MEMA)_n$, are illustrated in Figure 2.

For $(PEO_{45}MEMA)_n$, the ΔD versus Δf plot is relatively featureless. The dissipation initially increases linearly with decreasing frequency. However, as the adsorption proceeds toward equilibrium, the dissipation change levels off, demonstrating that the rigidity of the layer increases as the adsorption approaches the saturation value as also reported for this type of polymer in a previous report.[36] Recent studies of this polymer using dual polarization interferometry,[35] and the thickness of the layer determined in this study (2−3 nm, see Table 2 below) demonstrate that $(PEO_{45}MEMA)_n$ adsorbs with the long axis preferentially parallel to the surface.

The $\Delta D-\Delta f$ curve for $(METAC)_m$-*b*-$(PEO_{45}MEMA)_n$ initially follows that observed for the uncharged block. Thus, initially the diblock copolymer also adsorbs parallel to the surface. However, for the diblock copolymer, the dissipation increases rapidly again once the magnitude of the frequency change exceeds about 25 Hz, corresponding to a sensed mass of 1.3 mg/m^2. This transition point in the ΔD versus Δf curve corresponds to the transition point between the fast and slow

dx.doi.org/10.1021/la3028989 | *Langmuir* 2012, 28, 15537−15547

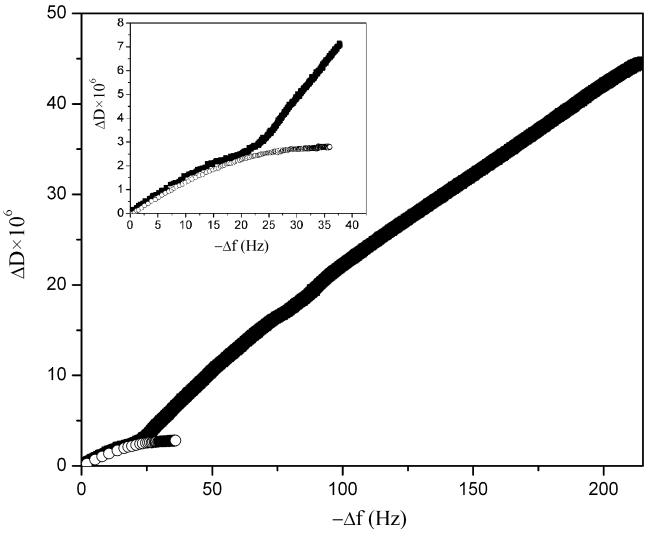

Figure 2. Dissipation change (ΔD) as a function of frequency change ($-\Delta f$) during adsorption of $(METAC)_m$-*b*-$(PEO_{45}MEMA)_n$ (upper curve) and $(PEO_{45}MEMA)_n$ (lower curve) on silica from a solution with a polymer concentration of 50 ppm in pure water. The inset shows the data in the range of $-\Delta f$ up to 40 Hz in more detail.

Table 2. Adsorbed Mass (Γ_{refl}) and Sensed Mass ($\Gamma_{QCM\text{-}D}$) for $(METAC)_m$, $(PEO_{45}MEMA)_n$, and $(METAC)_m$-*b*-$(PEO_{45}MEMA)_n$ as Well as Some Other Characteristics of the Layers Formed on Silica in Contact with Pure Water (pH ∼ 6) at 22 °C

	$(METAC)_m$	$(PEO_{45}MEMA)_n$	$(METAC)_m$-*b*-$(PEO_{45}MEMA)_n$
Γ_{refl}(mg/m^2)	0.17 ± 0.01	0.94 ± 0.05	2.75 ± 0.2
$\Gamma_{QCM\text{-}D}$ (mg/m^2)	0.4 ± 0.02	2.15 ± 0.2	48.6 ± 0.3
water content (wt%)	57.5 ± 0.5	56 ± 0.5	94.5 ± 0.2
μ_f (Pa)		(2.5 ± 0.1) × 10^5	(2.5 ± 0.2) × 10^5
η_f(Pa·s)		(2.2 ± 0.3) × 10^{-3}	(4.1 ± 0.3) × 10^{-3}
d_{eff} (nm)	0.4 ± 0.03	2.1 ± 0.3	48 ± 1
d_{Voigt} (nm)		2.8 ± 0.1	46 ± 2

adsorption regime illustrated in Figure 1. The data suggest that the transitions observed in Figures 1 and 2 are due to a change in polymer orientation from preferentially parallel to the surface at low coverage to significantly more extended conformations at high coverage.

3.2. Equilibrium Layer Properties. We now turn our attention to the properties of the $(METAC)_m$-*b*-$(PEO_{45}MEMA)_n$ layer that is formed once the adsorption plateau has been reached, and compare them to those obtained by adsorption of each block separately. To facilitate this comparison, the adsorption of the bottle-brush block, $(PEO_{45}MEMA)_n$, and that of the cationic block, $(METAC)_m$, was investigated at a concentration of 50 and 1 ppm, respectively. The low concentration for $(METAC)_m$ was chosen such that the number of charged groups added to the solution was similar to that for the diblock copolymer at a concentration of 50 ppm. The results obtained by means of optical reflectometry and QCM-D are summarized in Table 2.

In low ionic strength solutions, high charge density polyelectrolytes adsorb to oppositely charged surfaces in an amount that closely matches the surface charge density of the substrate in the presence of the adsorbed polyelectrolyte.[37] This is a consequence of the predominance of electrostatic forces. In our case, the adsorbed amount for the cationic block on silica was found to be 0.17 mg/m^2, which corresponds to 7.9 × 10^{17} cationic charges m^{-2}. This latter value also corresponds closely to the number of deprotonized silanol groups on the surface in the presence of the adsorbed polyelectrolyte. We note that the sensed mass determined by QCM-D for $(METAC)_m$ is significantly larger than the adsorbed mass, and this is primarily due to water molecules residing between the adsorbed polyelectrolytes.[38]

The uncharged bottle-brush block adsorbs to about 0.94 mg/m^2, which corresponds to 2.7 × 10^{17} PEO_{45} side chains m^{-2}. A similar, but slightly lower adsorbed amount, 0.70 mg/m^2, has been reported for a structurally similar polymer.[39]

The adsorbed amount found for $(METAC)_m$-*b*-$(PEO_{45}MEMA)_n$ was 2.75 ± 0.2 mg/m^2, significantly larger than for any of the two blocks separately. The number of charged groups in the layer is estimated to be 6.9 × 10^{17} m^{-2}, and the number of PEO_{45} side chains is estimated to be 7.4 × 10^{17} m^{-2}. These values were calculated using the number average of the block lengths, i.e., m = 90, n = 102 in $(METAC)_m$-*b*-$(PEO_{45}MEMA)_n$. There is a relatively large uncertainty in these values due to the polydispersity of the nonionic block. If, as would be expected, high molecular weight species were preferentially adsorbed,[23] then the number of charged segments brought to the surface by the diblock copolymer would be lower, and the number of PEO_{45} side chains would be higher than the values provided above. Considering these aspects, we draw the following conclusions: (i) the number of charges brought to the surface region by adsorption of $(METAC)_m$-*b*-$(PEO_{45}MEMA)_n$ is rather similar but somewhat lower than that found for $(METAC)_m$, indicating that steric rather than electrostatic interactions limits the adsorption, and (ii) the number of PEO_{45} side chains in the surface region is significantly larger for $(METAC)_m$-*b*-$(PEO_{45}MEMA)_n$ than for $(PEO_{45}MEMA)_n$.

The adsorbed layers formed by $(PEO_{45}MEMA)_n$, and $(METAC)_m$-*b*-$(PEO_{45}MEMA)_n$ displayed a sufficient high dissipation value to allow the data to be analyzed using the Voigt model. The data analysis provides information on shear viscosity, shear elasticity, and relaxation time, as well as layer thickness, and these data are provided in Table 2. The layer thickness can also be determined from the adsorbed and sensed mass as described by eq 13. We note that the two methods used for determining the layer thickness provides consistent results. For instance, for the diblock copolymer, a layer thickness of 46 nm is suggested by the Voigt analysis, and a value of 48 nm is obtained by employing eq 13. The large thickness of the diblock copolymer layer, compared to the 3 nm cross-section radius of gyration of the bottle-brush block as determined by SANS[40] and SAXS,[41] evidence that a layer structure where the backbone of the bottle-brush block is oriented preferentially perpendicular to the surface has been achieved. The large thickness of the layer further indicates that the terminal PEO_{45} side chains are directed preferentially toward the solution and not parallel to the surface, as would be expected due to excluded volume effects. The thickness value is also likely amplified by preferential adsorption of high molecular weight block copolymers.

The layer formed by $(METAC)_m$-*b*-$(PEO_{45}MEMA)_n$ was also imaged in water using AFM and the PeakForce QNM tapping mode (for details see Supporting Information). The image provided in the Supporting Information (Figure S5) is

dx.doi.org/10.1021/la3028989 | Langmuir 2012, 28, 15537−15547

rather featureless, but shows that the diblock copolymer completely covers the silica surface. The RMS roughness over a $2 \times 2\ \mu m^2$ surface area is small, about 0.4 nm. This value corresponds to the roughness of the layer under high compression and does not reflect the fact that in uncompressed state different chains are likely to protrude to different extent from the surface

3.3. Effect of Ionic Strength on Adsorption. From the data presented in section 3.2, it is clear that primarily the cationic block anchors $(METAC)_m$-*b*-$(PEO_{45}MEMA)_n$ to the silica surface. Thus, it is of relevance to consider how a change in ionic strength affects the adsorption, and this is elucidated in this section. It is well established that an increase in ionic strength of the solution will decrease the repulsion between segments within a polyelectrolyte, and decrease the electrostatic affinity to an oppositely charged surface. It has been shown that if only electrostatic forces dictate the adsorption, then the adsorbed amount will decrease with increasing ionic strength.[42] However, in our case, both electrostatic and nonelectrostatic forces are of importance, as evidenced by the significant adsorption of the nonionic block. Thus, it is not a priori clear how a change in ionic strength will affect adsorption. To elucidate this adsorption of $(METAC)_m$-*b*-$(PEO_{45}MEMA)_n$ from aqueous NaCl, solutions of different concentrations were investigated by means of optical reflectometry and QCM-D. The results are reported in Figure 3.

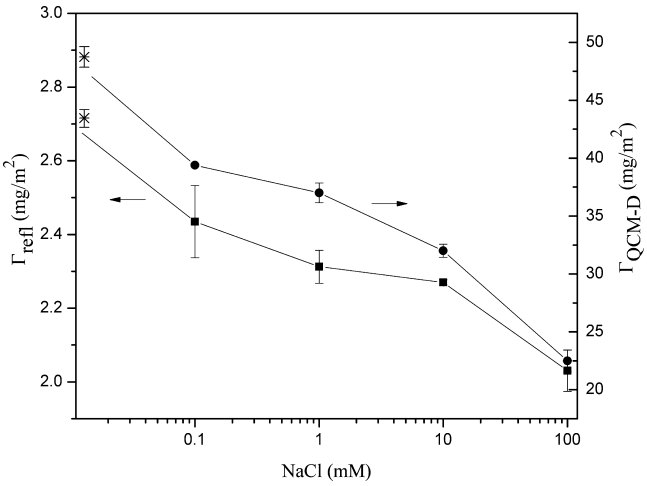

Figure 3. Adsorbed amount (Γ_{refl}(■)) and sensed mass (Γ_{QCM-D}(●)) of $(METAC)_m$-*b*-$(PEO_{45}MEMA)_n$ on silica as a function of NaCl concentration. The points marked with "*" are obtained with no added salt. The concentration of the diblock copolymer was 50 ppm, pH ~ 6, and the temperature 22 °C. The error bars correspond to standard deviations from three measurements.

The main finding is that the adsorbed amount decreases with ionic strength, from about 2.75 mg/m^2 in water to about 2.1 mg/m^2 in 100 mM NaCl. The sensed mass decreases similarly with increasing ionic strength (see Figure 3). The QCM-D data were also modeled within the Voigt viscoelastic framework, and the results show that the thickness of the layer decreases significantly with increasing ionic strength. The same conclusion is reached when the thickness is calculated from eq 13 (Figure 4). We attribute the reduced layer thickness to the reduced adsorbed amount, which lowers the repulsion between the extended bottle-brush blocks. The alternative interpretation that addition of NaCl reduces the solvent quality

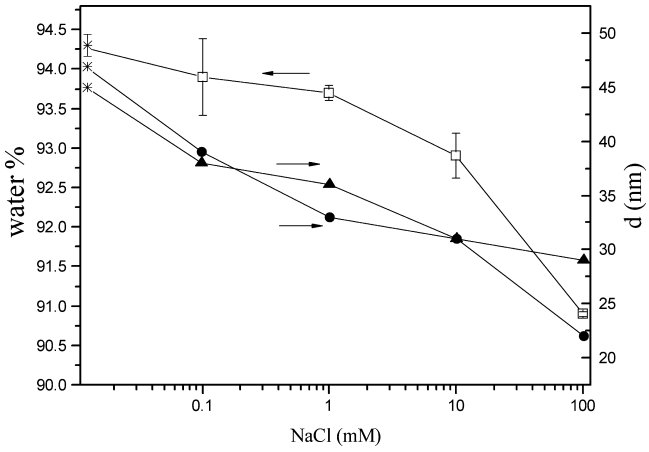

Figure 4. Water content of $(METAC)_m$-*b*-$(PEO_{45}MEMA)_n$ layers formed by adsorption from water (∗) and NaCl solutions of different concentrations (□). Thickness of the layer calculated by eq 13 (●) and from the Vogit model (▲), the thickness of the layer after rinse with water (∗).

for PEO and causes shrinkage of the layer is disregarded since 100 mM NaCl hardly affects the cloud point of PEO.[43] The reduced layer thickness at higher ionic strengths also results in decreased water content of the layer (Figure 4).

The water content of the adsorbed layer, as provided in Figure 4, was calculated from eq 12. Clearly, the water content is very large, above 94 wt %, for the layer adsorbed from water, decreasing to about 91 wt % for the layer formed from 100 mM NaCl solution. For comparison, the water content of layers formed by *random* bottle-brush copolymers are somewhat lower, varying between 90 and 80 wt % depending on the side-chain density.[39] Further, the water content in the ethylene oxide (EO) region in adsorbed layers of ethoxylated surfactants has been estimated to 77 vol%.[12] The direct hydration of the EO groups has been estimated by NMR spectroscopy, and found to amount to 2−6 water molecules per EO group.[44,45] This corresponds to a water content in the range 55−71 wt %. The significantly higher water content found in this study, 94−91 wt % corresponds to about 40−25 water molecules per EO group, which leads to the conclusion that it is water molecules residing between the PEO_{45} side chains rather than direct hydration of the EO groups that contributes most significantly to the high water content of the $(METAC)_m$-*b*-$(PEO_{45}MEMA)_n$ layers.

3.4. Desorption of Preadsorbed Layers. In this section we, like in the previous section, explore ionic strength effects, but we now consider how a layer of $(METAC)_m$-*b*-$(PEO_{45}MEMA)_n$ formed by adsorption from water is affected by rinsing with NaCl solutions of different ionic strengths. In these rinsing steps, no polymers are present in solution. The results obtained with optical reflectometry and QCM-D are provided in Figure 5.

Rinsing with water results in no detectable change in the adsorbed amount or sensed mass. However, as the salt concentration is increased ,some desorption is noted, and more clearly so in the adsorbed amount than in the sensed mass. The lower response observed in the QCM measurements is due to replacement of polymer in the layer with hydrodynamically trapped water that also contributes to the sensed mass.

dx.doi.org/10.1021/la3028989 | *Langmuir* 2012, 28, 15537−15547

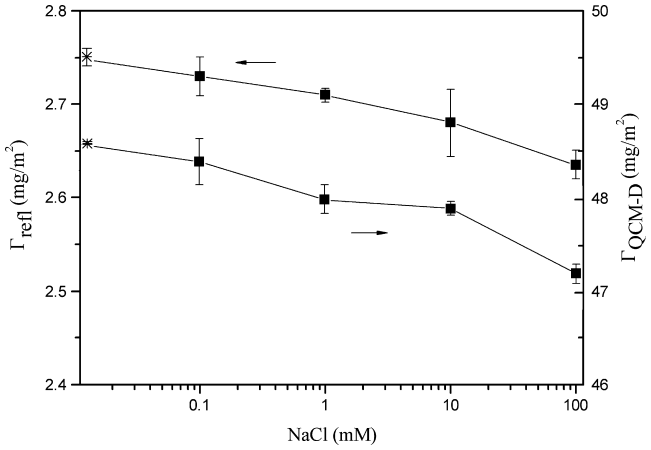

Figure 5. Adsorbed amount and sensed mass of $(METAC)_m$-*b*-$(PEO_{45}MEMA)_n$ layers after rinsing with NaCl solutions of different concentrations. The polymer was initially adsorbed from a 50 ppm aqueous solution at pH ∼ 6 (∗), and then the layer was subsequently rinsed with polymer-free solutions of increasing NaCl concentration (■).The rinse time at each NaCl concentration was about 30 min.

The lowest adsorbed amount, still above 2.7 mg/m^2, was obtained after soaking the surfaces in 100 mM NaCl. This is significantly larger than the about 2.1 mg/m^2, obtained by adsorbing the diblock copolymer directly from a 100 mM NaCl solution. Consistently, the sensed mass of the layer formed from water and then exposed to 100 mM NaCl is significantly larger than the sensed mass of the layer formed directly from 100 mM NaCl. A separate experiment was performed to test the long-term stability of the diblock copolymer layer adsorbed from water. The layer was rinsed with 100 mM NaCl and left in this solution for 48 h. No further desorption above that indicated in Figure 5 was observed. Thus, once adsorbed, the $(METAC)_m$-*b*-$(PEO_{45}MEMA)_n$ layer is resistant to significant desorption even at relatively high NaCl concentrations (at least up to 100 mM).

3.5. Surface Forces and Friction. We have now established that $(METAC)_m$-*b*-$(PEO_{45}MEMA)_n$ adsorb to silica and form an electrostatically anchored branched brush layer with large thickness and high water content, and that the layer is resistant to desorption even in 100 mM NaCl. In this section, we describe normal and friction forces between such layers as measured by using the AFM colloidal probe technique. The results are shown in Figure 6.

The forces acting between silica surfaces coated with adsorbed $(METAC)_m$-*b*-$(PEO_{45}MEMA)_n$ layers are long-range and purely repulsive on both approach and retraction. The most long-range part of the force curve is due to double-layer repulsion, whereas a steric repulsion dominates at distances below 40 nm. No hard wall contact is reached at the highest force applied in this study (F_n/R = 2 mN/m). The same forces are measured on approach and separation, and we conclude that $(METAC)_m$-*b*-$(PEO_{45}MEMA)_n$ layers provide steric stabilization.

The friction force between silica surfaces across water is shown as a function of load in Figure 6b. The friction increases close to linearly with applied load, and the friction coefficient is about 0.25. By contrast, the friction force between silica surfaces coated with an adsorbed layer of $(METAC)_m$-*b*-$(PEO_{45}MEMA)_n$ layer is significantly smaller. The friction force law does not follow Amontons' law, but increases slightly more than in proportion to the load. At the highest load applied in this study, 260 nN corresponding to a pressure of about 60 MPa, the effective friction coefficient $\mu_{eff} = F_f/F_n$ amounts to 0.04. Thus, it is clear that the novel diblock bottle-brush polymer structure offers low friction and high load bearing capacity in aqueous solutions.

4. DISCUSSION

In the discussion we focus on four points. First we consider the formation of the $(METAC)_m$-*b*-$(PEO_{45}MEMA)_n$ layer on silica, and the evidence pointing to significant structural changes during the build-up process. In the following two sections we

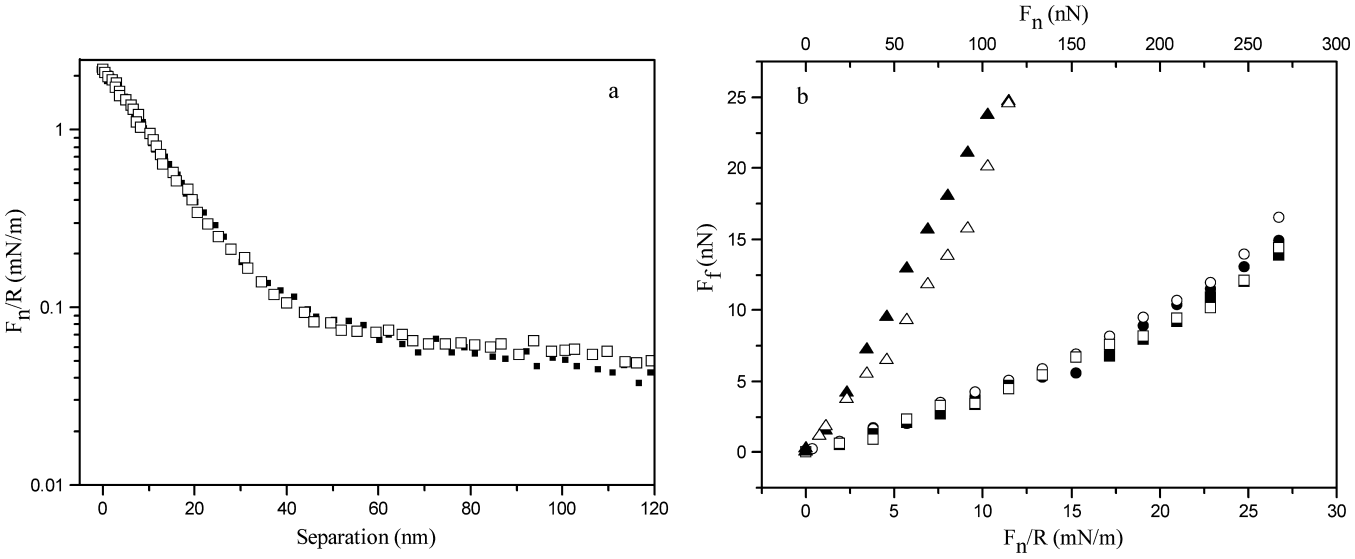

Figure 6. (a) Force normalized by radius between silica surfaces coated with an adsorbed $(METAC)_m$-*b*-$(PEO_{45}MEMA)_n$ layer across a 50 ppm solution of the diblock copolymer as a function of separation. Filled and unfilled symbols represent data obtained on approach and retraction, respectively. (b) Friction force versus load for two uncoated silica surfaces across water (triangles), and for silica coated with an adsorbed $(METAC)_m$-*b*-$(PEO_{45}MEMA)_n$ layer across a 50 ppm solution of the diblock copolymer (circles). Filled and unfilled symbols represent data obtained on loading and unloading, respectively.

dx.doi.org/10.1021/la3028989 | *Langmuir* 2012, 28, 15537−15547

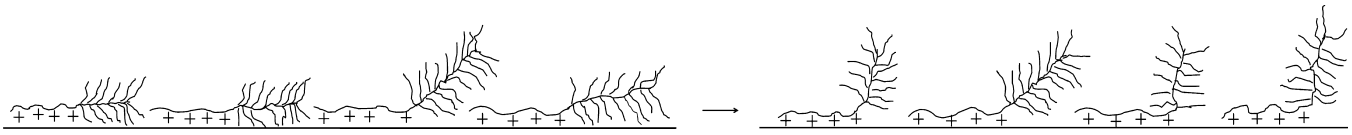

Figure 7. Schematic illustration of the time evolution of the structure of $(METAC)_m$-*b*-$(PEO_{45}MEMA)_n$ during the adsorption process. We note that the Rg of the cross-section of the bottle-brush block in solutions is about 3 nm,[40,41] and thus the side chains are more coiled than illustrated in this simple sketch.

consider ionic strength effects, first on the adsorption process and then on the desorption process of preformed layers. In the final section of the discussion we highlight the differences in the adsorbed layer structure of the diblock copolymer $(METAC)_m$-*b*-$(PEO_{45}MEMA)_n$ in comparison to those of structurally similar random copolymers.

4.1. Build-Up of the Layer Formed by the $(METAC)_m$-*b*-$(PEO_{45}MEMA)_n$ Diblock Copolymer. Both blocks of $(METAC)_m$-*b*-$(PEO_{45}MEMA)_n$ have affinity for the silica surface as evidenced by the adsorption data for the individual blocks (Table 2). However, the affinity to the silica surface is different for the two blocks, and a preferential accumulation of charged segments at the surface is expected when equilibrium is approached.[20]

It is significant that the $\Delta D-\Delta f$ plot for the diblock copolymer initially follows that obtained for the uncharged bottle-brush block (Figure 2), and it demonstrates that the initial adsorption occurs with a preferential orientation parallel to the surface (Figure 7). However, as adsorption proceeds, cationic segments are replacing PEO segments at the surface, and this results in a transformation of the layer structure where the cationic segments are accumulated at the surface and the PEO bottle-brush chains are extended away from the surface. Indeed, this structure has been predicted by lattice mean field calculations[20] and suggests the formation of a surface anchored branched brush layer as sketched in Figure 7.

It is of some interest to compare the shear viscosity and shear elasticity data in the 15 MHz range reported in Table 2, with similar data reported in the literature. The values obtained for the uncharged block are similar to those reported for the same polymer structure by Iruthayaraj et al.[36] The random block copolymer investigated by Iruthayaraj et al. that formed the most extended polymer layer, thickness about 20 nm, have a lower shear viscosity and higher shear elasticity than observed for our diblock copolymer that formed a significantly thicker, 46–48 nm, layer.[36] The high water content in our layer rationalizes the lower shear elasticity, whereas the larger thickness is suggested to explain the higher shear viscosity, since for a constant thickness the shear viscosity decreases with increasing water content.[46]

4.2. Effect of Ionic Strength on the Adsorption of $(METAC)_m$-*b*-$(PEO_{45}MEMA)_n$. The effect of ionic strength on the adsorbed and sensed mass of $(METAC)_m$-*b*-$(PEO_{45}MEMA)_n$ is illustrated in Figure 3. Both of these quantities decrease with increasing ionic strength. It is well-known that an increase in ionic strength results in screening of electrostatic forces. This leads to (i) a decreased electrostatic affinity between the cationic block and the silica surface, (ii) a decreased repulsion between the cationic blocks, (iii) an increased silica surface charge density,[47] (iv) a decreased affinity between the PEO bottle-brush block and silica as a consequence of the increased surface charge density,[47] and (v) a change in conformation of the cationic block in solution toward a more coiled state.

Of these effects, numbers (i) and (iv) favor a decreased adsorption with increasing ionic strength, whereas factors (ii) and (iii) favor increased adsorption. It is more difficult to judge how the change in polymer conformation (factor v) will affect the adsorption. On the basis of the observation that an increase in ionic strength leads to a decrease in the adsorbed amount, we conclude that factors (i) and (iv) are most important in our case.

4.3. Effect of Ionic Strength on Preadsorbed Layers of $(METAC)_m$-*b*-$(PEO_{45}MEMA)_n$. The effect of ionic strength on preadsorbed layers of $(METAC)_m$-*b*-$(PEO_{45}MEMA)_n$ is illustrated in Figure 5. In general, the effect is rather small with a tendency of some limited desorption at higher ionic strengths. This suggests that the structure of the layer, once it has been formed, remains almost unchanged during rinsing and exposure to salt solutions with different ionic strengths, and this was indeed confirmed by our experiments that lasted for 48 h.

Desorption of a polymer from a surface can be viewed as being due to two consecutive steps. First the polymer detaches from the surface and resides close to the surface (in the subsurface region). Next, the polymer diffuses away from the surface due to the concentration gradient existing between the subsurface region and the bulk solution.[48] For polymers showing a high affinity to the surface, the subsurface concentration is always low, and the concentration gradient and consequently the driving force for transport to the bulk will be low. As first suggested by Cohen Stuart at al., this rationalizes why polymer adsorption often is practically irreversible with respect to dilution.[48]

The situation is more complex when the solution conditions are changed during rinsing, as when the ionic strength was varied during the desorption step (Figure 5). We may now have a situation where the polymers in the subsurface region are repelled from the surface, which would provide another driving force for the transport to bulk solution. This is part of the reason why some desorption is observed at high ionic strength in our case. The other reason is that the electrostatic affinity for $(METAC)_m$-*b*-$(PEO_{45}MEMA)_n$ to the surface decreases and this facilitates the first step of the desorption process: detachment from the surface to the subsurface region. The low desorption observed, even in 100 mM NaCl solutions, is a consequence of the large number of segments that bind to the surface with high electrostatic affinity, which makes complete detachment an unlikely event. A practical consequence of this finding is that an enhanced adsorbed amount of $(METAC)_m$-*b*-$(PEO_{45}MEMA)_n$ in high ionic strength solutions can be achieved by allowing adsorption to proceed at low ionic strength and then increase the salt concentration rather than allowing the layer to form at the higher ionic strength. This approach relies on the formation of long-lived trapped states rather than equilibrium considerations.

4.4. Comparison with Random Bottle-Brush Polymers. Bottle-brush polymers consisting of a random sequence of cationic segments and segments carrying nonionic hydrophilic

dx.doi.org/10.1021/la3028989 | *Langmuir* 2012, 28, 15537–15547

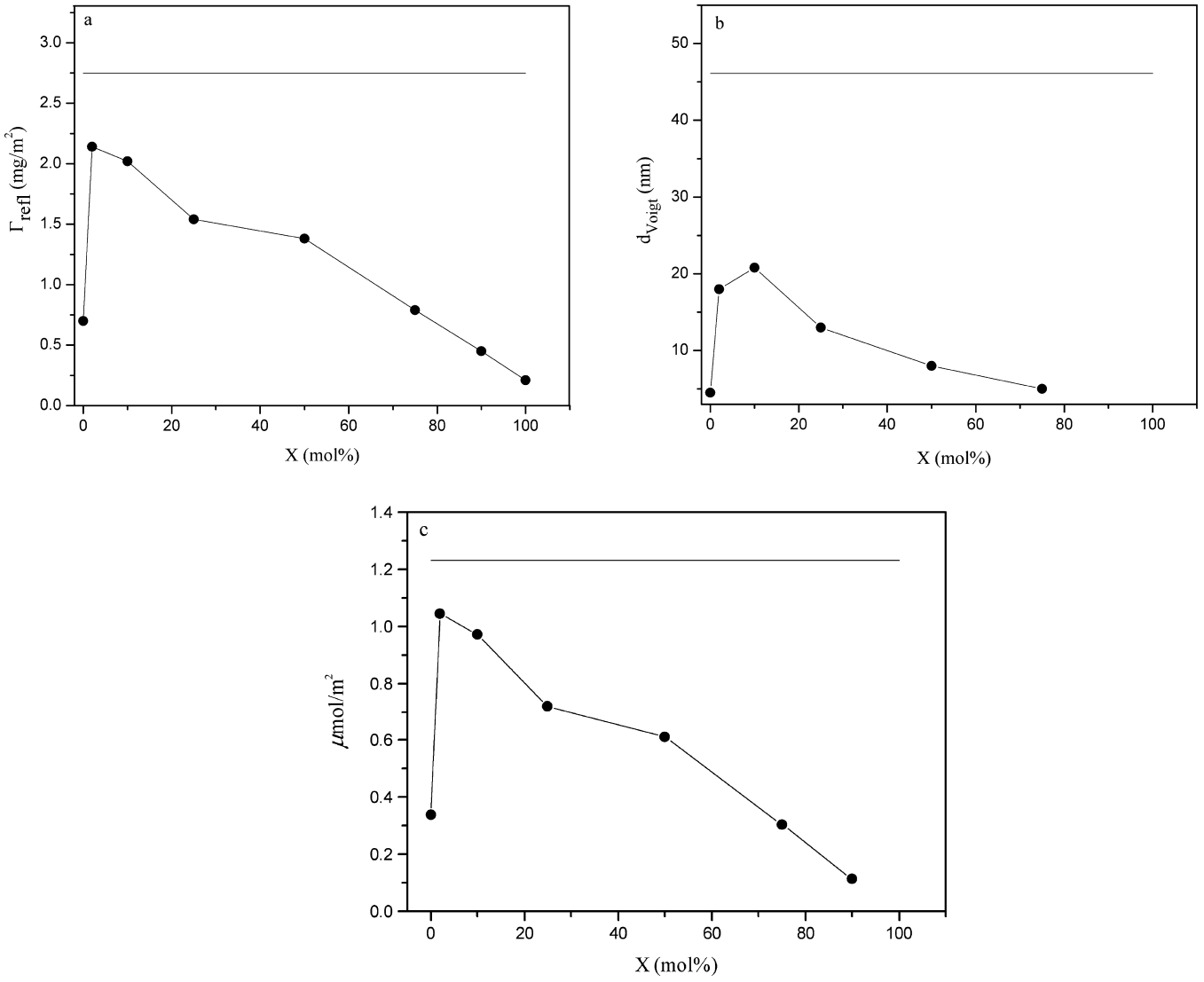

Figure 8. (a) Adsorbed amount, (b) layer thickness, and (c) number of PEO_{45} side chains m^{-2} for PEO_{45}MEMA:METAC-X (symbols) compared to that obtained for $(METAC)_m$-*b*-$(PEO_{45}MEMA)_n$ (horizontal lines) as a function of mol % charged segments in the random copolymers. Data for the random copolymers are from refs 36 and 39.

side chains have received great interest in recent years due to, e.g., favorable lubrication properties[10,11,49] and low nonspecific protein adsorption.[17−19] The diblock copolymer, $(METAC)_m$-*b*-$(PEO_{45}MEMA)_n$ considered in this study has the same charged segment (METAC) and the same uncharged segment with PEO_{45} side chain (PEO_{45}MEMA) as the random copolymers, PEO_{45}MEMA:METAC-X, studied previously. The "X" in PEO_{45}MEMA:METAC-X denotes the mol % of charged segments in the random copolymer. The two polymer types also have similar molecular weight. The adsorbed amount, layer thickness, and number of PEO_{45} side chains per unit are achieved by adsorption of the random copolymers, as a function of the mol % charged main-chain segments, and are compared with that obtained by adsorption of $(METAC)_m$-*b*-$(PEO_{45}MEMA)_n$ in Figure 8.

Clearly, the adsorbed amount and the number of PEO_{45} side chains at the interface achieved by adsorption of the $(METAC)_m$-*b*-$(PEO_{45}MEMA)_n$ diblock copolymer is substantially larger than that obtained by any of the random copolymers. Even more striking is the much larger thickness of the diblock copolymer layer compared to that of random copolymer layers. This is a consequence of the larger degree of segregation of the charged and uncharged segments in the diblock copolymer layer, as recently predicted by lattice mean-field calculations.[20]

Low friction forces have been achieved with random bottle-brush copolymers having the same side chains as $(METAC)_m$-*b*-$(PEO_{45}MEMA)_n$, and friction coefficients as low as 0.006 could be achieved up to pressures of about 30 MPa.[10] Interestingly, this low friction coefficient was obtained between extended layers forming structures similar to the branched-brush architecture obtained for $(METAC)_m$-*b*-$(PEO_{45}MEMA)_n$. In this work, we show that low friction forces and a high load bearing capacity of at least 60 MPa can be achieved with this diblock bottle-brush copolymer. Further details on the friction properties offered by $(METAC)_m$-*b*-$(PEO_{45}MEMA)_n$ will be reported in a forthcoming publication.

5. CONCLUSIONS

We have, based on predictions from lattice mean-field calculations,[20] designed and synthesized a diblock copolymer consisting of a linear cationic block and a nonionic bottle-brush

dx.doi.org/10.1021/la3028989 | *Langmuir* 2012, 28, 15537−15547

block with 45 units-long PEO side chains. In agreement with theoretical predictions, we find that the diblock copolymer, $(METAC)_m$-*b*-$(PEO_{45}MEMA)_n$, adsorbs to larger quantities and forms thicker layers than random bottle-brush polymers containing the same segments.[36] Adsorption from water results in an adsorbed amount of 2.75 ± 0.2 mg/m^2 and a layer thickness of 46−48 nm. The water content of the layer is high, above 90 wt %.

The adsorbed amount decreases with increasing ionic strength of the solution from which the layer is formed. In contrast, *preadsorbed* layers of $(METAC)_m$-*b*-$(PEO_{45}MEMA)_n$ formed from salt-free aqueous solutions display a low sensitivity to the ionic strength of the solution used for rinsing the surface. This demonstrates the importance of long-lived trapped states and offers a practical means for achieving high adsorbed amounts in high ionic strength solutions. Kinetic studies demonstrate that the polymer initially adsorbs parallel to the surface, but as the adsorption proceeds, cationic segments displace uncharged segments at the surface. As a result, a thick, branched brush-like layer with a high content of 45 units-long PEO) side-chains is formed. This layer offers strong steric repulsion, low friction forces, and high load bearing capacity.

■ ASSOCIATED CONTENT

Supporting Information

Additional experimental details. This material is available free of charge via the Internet at http://pubs.acs.org.

■ AUTHOR INFORMATION

Corresponding Author

*Mailing address: Surface and Corrosion Science, KTH Royal Institute of Technology, Drottning Kristinas väg 51, SE-100 44 Stockholm, Sweden. E-mail: esben@kth.se.

Notes

The authors declare no competing financial interest.

■ ACKNOWLEDGMENTS

X.L. acknowledges a stipend from the Chinese Scholarship Council (CSC), P.C. and M.R. acknowledge financial support from VR. The project was carried out within the framework of the SSF program "Microstructure, Corrosion and Friction Control". C.V. and R.M. gratefully acknowledge financial support from the Research Council of Lithuania under the project MIP-50/2010. Lubica Macakova at the Institute for Surface Chemistry, YKI, is thanked for valuable discussions.

■ REFERENCES

(1) Dedinaite, A. Biomimetic Lubrication. *Soft Matter* **2012**, *8*, 273−284.
(2) *Encyclopedia of Surface and Colloid Science*, 2nd ed.; Taylor & Francis: New York, 2010.
(3) Di Cola, E.; Yakubov, G. E.; Waigh, T. A. Double-Globular Structure of Porcine Stomach Mucin: A Small-Angle X-ray Scattering Study. *Biomacromolecules* **2008**, *9*, 3216−3222.
(4) Chang, D. P.; Abu-Lail, N. I.; Guilak, F.; Jay, G. D.; Zauscher, S. Conformational Mechanics, Adsorption, and Normal Force Interactions of Lubricin and Hyaluronic Acid on Model Surfaces. *Langmuir* **2008**, *24*, 1183−1193.
(5) Jones, A. R. C.; Gleghorn, J. P.; Hughes, C. E.; Fitz, L. J.; Zollner, R.; Wainwright, S. D.; Caterson, B.; Morris, E. A.; Bonassar, L. J.; Flannery, C. R. Binding and Localization of Recombinant Lubricin to Articular Cartilage Surfaces. *J. Orthop. Res.* **2007**, *25*, 283−292.
(6) Argüeso, P.; Gipson, I. K. Epithelial Mucins of the Ocular Surface: Structure, Biosynthesis and Function. *Exp. Eye Res.* **2001**, *73*, 281−289.
(7) Singh, P. K.; Hollingsworth, M. A. Cell Surface-Associated Mucins in Signal Transduction. *Trends Cell Biol.* **2006**, *16*, 467−476.
(8) Horkay, F.; Basser, P. J.; Hecht, A.-M.; Geissler, E. Gel-like Behavior in Aggrecan Assemblies. *J. Chem. Phys.* **2008**, *128* (135103), 1−7.
(9) Seror, J.; Merkher, Y.; Kampf, N.; Collinson, L.; Day, A. J.; Maroudas, A.; Klein, J. Articular Cartilage Proteoglycans As Boundary Lubricants: Structure and Frictional Interaction of Surface-Attached Hyaluronan and Hyaluronan−Aggrecan Complexes. *Biomacromolecules* **2011**, *12*, 3432−3443.
(10) Pettersson, T.; Naderi, A.; Makuska, R. a.; Claesson, P. M. Lubrication Properties of Bottle-Brush Polyelectrolytes: An AFM Study on the Effect of Side Chain and Charge Density. *Langmuir* **2008**, *24*, 3336−3347.
(11) Drobek, T.; Spencer, N. D. Nanotribology of Surface-Grafted PEG Layers in an Aqueous Environment. *Langmuir* **2007**, *24*, 1484−1488.
(12) Claesson, P. M.; Kjellin, M.; Rojas, O. J.; Stubenrauch, C. Short-Range Interactions between Non-ionic Surfactant Layers. *Phys. Chem. Chem. Phys.* **2006**, *8*, 5501−5514.
(13) Tyrode, E.; Johnson, C. M.; Rutland, M. W.; Claesson, P. M. Structure and Hydration of Poly(ethylene oxide) Surfactants at the Air/Liquid Interface. A Vibrational Sum Frequency Spectroscopy Study. *J. Chem. Phys. C* **2007**, *111*, 11642−11652.
(14) Kjellander, R.; Florin, E. Water Structure and Changes in Thermal Stability of the System Poly(ethylene oxide)−Water. *J. Chem. Soc., Faraday Trans.* **1981**, *77*, 2053−2077.
(15) Claesson, P. M.; Gölander, C.-G. Direct Measurements of Steric Interactions between Mica Surfaces Covered with Electrostatically Bound Low-Molecular-Weight Polyethylene Oxide. *J. Colloid Interface Sci.* **1987**, *117*, 366−374.
(16) Silvander, M., Steric Stabilization of Liposomes — A Review. In *Lipid and Polymer−Lipid Systems*; Nylander, T., Lindman, B., Eds.; Springer: Berlin/Heidelberg, 2002; Vol. *120*, pp 35−40.
(17) Olanya, G.; Thormann, E.; Varga, I.; Makuška, R.; Claesson, P. M. Protein Interactions with Bottle-Brush Polymer Layers: Effect of Side Chain and Charge Density Ratio Probed by QCM-D and AFM. *J. Colloid Interface Sci.* **2010**, *349*, 265−274.
(18) Pasche, S.; De Paul, S. M.; Vörös, J.; Spencer, N. D.; Textor, M. Poly(L-lysine)-*graft*-poly(ethylene glycol) Assembled Monolayers on Niobium Oxide Surfaces: A Quantitative Study of the Influence of Polymer Interfacial Architecture on Resistance to Protein Adsorption by ToF-SIMS and in Situ OWLS. *Langmuir* **2003**, *19*, 9216−9225.
(19) Zhou, Y.; Liedberg, B.; Gorochovceva, N.; Makuska, R.; Dedinaite, A.; Claesson, P. M. Chitosan-*N*-poly(ethylene oxide) Brush Polymers for Reduced Nonspecific Protein Adsorption. *J. Colloid Interface Sci.* **2007**, *305*, 62−71.
(20) Linse, P.; Claesson, P. M. Modeling of Bottle-Brush Polymer Adsorption onto Mica and Silica Surfaces. *Macromolecules* **2009**, *42*, 6310−6318.
(21) Linse, P.; Claesson, P. M. Modeling of Bottle-Brush Polymer Adsorption onto Mica and Silica Surfaces: Effect of Side-Chain Length. *Macromolecules* **2010**, *43*, 2076−2083.
(22) Fleer, G. J.; Cohen Stuart, M. A.; Scheutjens, J. M. H. M.; Cosgrove, T.; Vincent, B. *Polymers at Interfaces*; Chapman & Hall: New York, 1993.
(23) Schillén, K.; Claesson, P. M.; Malmsten, M.; Linse, P.; Booth, C. Properties of Poly(ethylene oxide)−Poly(butylene oxide) Diblock Copolymers at the Interface between Hydrophobic Surfaces and Water. *J. Phys. Chem. B* **1997**, *101*, 4238−4252.
(24) Dijt, J. C.; Stuart, M. A. C.; Fleer, G. J. Reflectometry as a Tool for Adsorption Studies. *Adv. Colloid Interface Sci.* **1994**, *50*, 79−101.
(25) Dabroś, T.; van de Ven, T. G. M. A Direct Method for Studying Particle Deposition onto Solid Surfaces. *Colloid Polym. Sci.* **1983**, *261*, 694−707.

(26) Dėdinaitė, A.; Bastardo, L. Interactions between Mucin and Surfactants at Solid−Liquid Interfaces. *Langmuir* **2002**, *18*, 9383−9392.
(27) Rodahl, M.; Hook, F.; Krozer, A.; Brzezinski, P.; Kasemo, B. Quartz Crystal Microbalance Setup for Frequency and *q*-Factor Measurements in Gaseous and Liquid Environments. *Rev. Sci. Instrum.* **1995**, *66*, 3924−3930.
(28) Sauerbrey, G. Verwendung von Schwingquarzen zur Wägung dünner Schichten und zur Mikrowägung. *Z. Phys. A: Hadrons Nucl.* **1959**, *155*, 206−222.
(29) Johannsmann, D.; Mathauer, K.; Wegner, G.; Knoll, W. Viscoelastic Properties of Thin Films Probed with a Quartz-Crystal Resonator. *Phys. Rev. B* **1992**, *46*, 7808.
(30) Rodahl, M.; Kasemo, B. On the Measurement of Thin Liquid Overlayers with the Quartz-Crystal Microbalance. *Sens. Actuators, A* **1996**, *54*, 448−456.
(31) Naderi, A.; Iruthayaraj, J.; Vareikis, A.; Maku ka, R.; Claesson, P. M. Surface Properties of Bottle-Brush Polyelectrolytes on Mica: Effects of Side Chain and Charge Densities. *Langmuir* **2007**, *23*, 12222−12232.
(32) Green, C. P.; Lioe, H.; Cleveland, J. P.; Proksch, R.; Mulvaney, P.; Sader, J. E. Normal and Torsional Spring Constants of Atomic Force Microscope Cantilevers. *Rev. Sci. Instrum.* **2004**, *75*, 1988−1996.
(33) Sader, J. E.; Chon, J. W. M.; Mulvaney, P. Calibration of Rectangular Atomic Force Microscope Cantilevers. *Rev. Sci. Instrum.* **1999**, *70*, 3967−3969.
(34) Pettersson, T.; Nordgren, N.; Rutland, M. W.; Feiler, A. Comparison of Different Methods to Calibrate Torsional Spring Constant and Photodetector for Atomic Force Microscopy Friction Measurements in Air and Liquid. *Rev. Sci. Instrum.* **2007**, *78*, 093702−8.
(35) Bijelic, G.; Shovsky, A.; Varga, I.; Makuska, R.; Claesson, P. M. Adsorption Characteristics of Brush Polyelectrolytes on Silicon Oxynitride Revealed by Dual Polarization Interferometry. *J. Colloid Interface Sci.* **2010**, *348*, 189−197.
(36) Iruthayaraj, J.; Olanya, G.; Claesson, P. M. Viscoelastic Properties of Adsorbed Bottle-Brush Polymer Layers Studied by Quartz Crystal Microbalance Dissipation Measurements. *J. Chem. Phys. C* **2008**, *112*, 15028−15036.
(37) Linse, P. Adsorption of Weakly Charged Polyelectrolytes at Oppositely Charged Surfaces. *Macromolecules* **1996**, *29*, 326−336.
(38) Lundin, M.; Macakova, L.; Dedinaite, A.; Claesson, P. Interactions between Chitosan and SDS at a Low-Charged Silica Substrate Compared to Interactions in the Bulk − The Effect of Ionic Strength. *Langmuir* **2008**, *24*, 3814−3827.
(39) Olanya, G.; Iruthayaraj, J.; Poptoshev, E.; Makuska, R.; Vareikis, A.; Claesson, P. M. Adsorption Characteristics of Bottle-Brush Polymers on Silica: Effect of Side Chain and Charge Density. *Langmuir* **2008**, *24*, 5341−5349.
(40) Bastardo, L. A.; Iruthayaraj, J.; Lundin, M.; Dedinaite, A.; Vareikis, A.; Makuška, R.; van der Wal, A.; Furó, I.; Garamus, V. M.; Claesson, P. M. Soluble Complexes in Aqueous Mixtures of Low Charge Density Comb Polyelectrolyte and Oppositely Charged Surfactant Probed by Scattering and NMR. *J. Colloid Interface Sci.* **2007**, *312*, 21−33.
(41) Dedinaite, A.; Bastardo, L. A.; Oliveira, C. L. P.; Pedersen, J. S.; Claesson, P. M.; Vareikis, A.; Makuška, R. Solution Properties of Bottle-Brush PolyelectrolytesIn *Proceedings of the Baltic Polymer Symposium*, Druskininkai, Lithuania, September 19−21, 2007.
(42) Van de Steeg, H. G. M.; Cohen Stuart, M. A.; De Keizer, A.; Bijsterbosch, B. H. Polyelectrolyte Adsorption: A Subtle Balance of Forces. *Langmuir* **1992**, *8*, 2538−2546.
(43) Bailey, F. E.; Callard, R. W. Some Properties of Poly(ethylene oxide)1 in Aqueous Solution. *J. Appl. Polym. Sci.* **1959**, *1*, 56−62.
(44) Nilsson, P. G.; Wennerstroem, H.; Lindman, B. Structure of Micellar Solutions of Nonionic Surfactants. Nuclear Magnetic Resonance Self-Diffusion and Proton Relaxation Studies of Poly-(ethylene oxide) Alkyl Ethers. *J. Phys. Chem.* **1983**, *87*, 1377−1385.
(45) Nilsson, P. G.; Lindman, B. Water Self-Diffusion in Nonionic Surfactant Solutions. Hydration and Obstruction Effects. *J. Phys. Chem.* **1983**, *87*, 4756−4761.
(46) Reimhult, E.; Larsson, C.; Kasemo, B.; Höök, F. Simultaneous Surface Plasmon Resonance and Quartz Crystal Microbalance with Dissipation Monitoring Measurements of Biomolecular Adsorption Events Involving Structural Transformations and Variations in Coupled Water. *Anal. Chem.* **2004**, *76*, 7211−7220.
(47) Iruthayaraj, J.; Poptoshev, E.; Vareikis, A.; Makuška, R. a.; van der Wal, A.; Claesson, P. M. Adsorption of Low Charge Density Polyelectrolyte Containing Poly(ethylene oxide) Side Chains on Silica: Effects of Ionic Strength and pH. *Macromolecules* **2005**, *38*, 6152−6160.
(48) Hoogeveen, N. G.; Cohen Stuart, M. A.; Fleer, G. J.; Böhmer, M. R. Formation and Stability of Multilayers of Polyelectrolytes. *Langmuir* **1996**, *12*, 3675−3681.
(49) Dedinaite, A.; Thormann, E.; Olanya, G.; Claesson, P. M.; Nystrom, B.; Kjoniksen, A.-L.; Zhu, K. Friction in Aqueous Media Tuned by Temperature-Responsive Polymer Layers. *Soft Matter* **2010**, *6*, 2489−2498.